Characterization and Solar Cell Application of GaSb Quantum Dots

Arthur Bowman, III
Physics, Wayne State University

NNIN iREU Site: National Institute for Materials Science (NIMS), Tsukuba, Ibaraki, Japan
NNIN iREU Principal Investigators: Dr. Takeshi Noda, High Efficiency Solar Cell Group, NIMS, Tsukuba, Ibaraki, Japan; Professor Hiroyuki Sakaki, Toyota Technological Institute, Nagoya, Aichi, Japan
NNIN iREU Mentor: Dr. Martin Elborg, High Efficiency Solar Cell Group, NIMS, Tsukuba, Ibaraki, Japan
Contact: abowmaniii@wayne.edu, noda.takeshi@nims.go.jp, elborg.martin@nims.go.jp

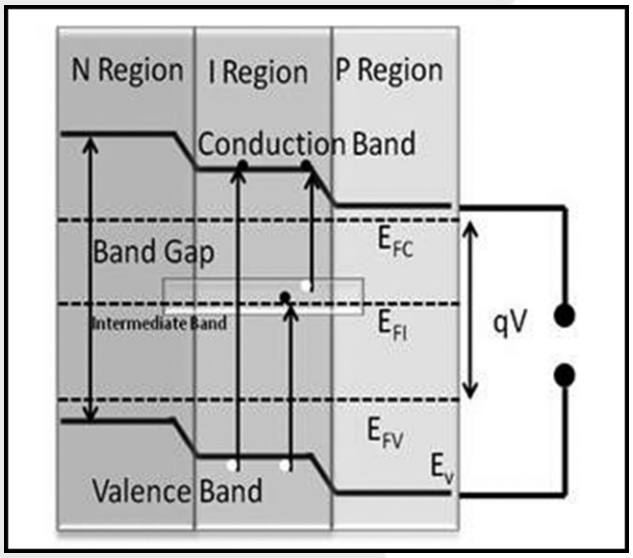

Figure 1: Ideal band diagram of the intermediate band solar cells.

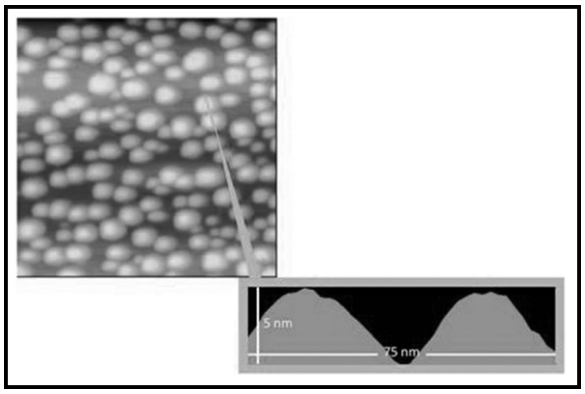

Figure 2: AFM micrograph of GaSb/AlGaAs QDs.

Introduction:

Intermediate band solar cells (IBSC) can potentially overcome the Shockley-Queisser (SQ) conversion efficiency limit of photovoltaic devices. In addition to photocurrent generated by photons above the band gap, IBSC can utilize a "two-step" photocurrent, wherein sub-bandgap photons excite carriers from the valence to intermediate band, then intermediate to conduction band, depicted schematically in Figure 1.

Quantum dot heterostructures (QDs) are one method of realizing intermediate energy states within the band gap. Our interest is in structures with type II band alignment. In contrast to commonly used type I structures, in which both electrons and holes are confined in the narrow bandgap material, radiative recombination can be largely suppressed in type-II structures, which would be preferable for solar cell application, because losses due to radiative recombination can be reduced.

QD solar cells realized from gallium antimonite (GaSb) embedded in gallium arsenide (GaAs) are of interest an example of type-II band solar cells. By changing the GaAs barrier to aluminum gallium arsenide (AlGaAs), we expect the dot energy levels will be situated deeply enough to achieve transition energies nearly matching the ideal IBSC configuration for highest efficiency proposed by Luque, et al. [1].

GaSb/GaAs QDs and GaSb/AlGaAs QDs were grown, and IBSC were fabricated using them. In this work, we determined the band alignment of GaSb/AlGaAs QDs, and then studied their solar cell applications.

Fabrication Procedure:

GaSb QDs embedded in GaAs and AlGaAs were grown on n-type GaAs <100> substrates using molecular beam epitaxy. We employed the Stranski-Krastanov growth mode, wherein growth is first layer by layer until the thickness reaches a critical value and growth continues through the coalescence of three-dimensional "islands." Ten layers of QDs were separated by 20 nm thick barrier layers to decouple adjacent electronic states. We fabricated QD solar cells using photolithography and sputtering. A phosphoric acid, hydrogen peroxide, and water etch was used to electrically decouple the devices. Gold wires were then bonded from the device to a serial package.

Results:

Atomic force microscopy (AFM) revealed the average height of GaSb QDs (Figure 2) was 5 nm, regardless of barrier material. The density of GaSb/GaAs QD layers was $2.9 \times 10^{10}/cm^2$ and 5.6×10^{10} $/cm^2$ for GaSb/AlGaAs QDs. Photoluminescence

PHYS

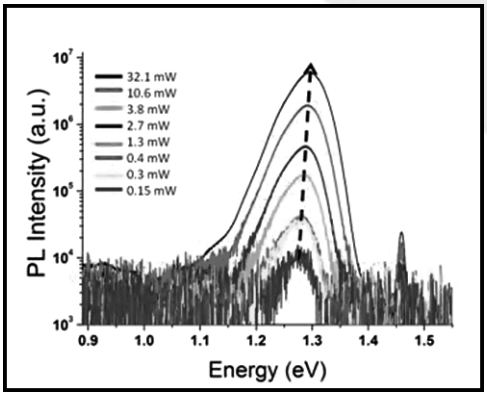

Figure 3: Blueshift of PL from GaSb/AlGaAs QDs with increasing laser power. (See full color version on page xxxvi.)

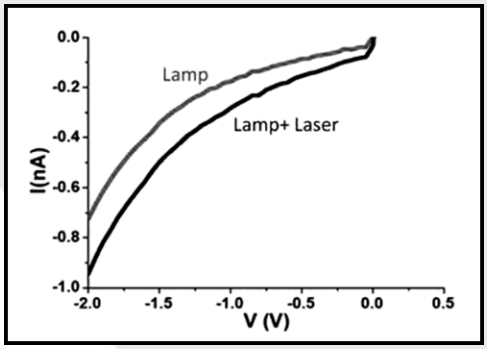

Figure 4: Two-step photocurrent generated by GaSb/AlGaAs QD solar cell.

(PL) measurements at 10 K revealed transitions at 1.09 eV for GaSb/GaAs QDs and 1.29 eV for GaSb/AlGaAs QDs from carriers occupying the QD layers. Hodgson, et al. [2] showed that increasing laser power results in a blueshift of the peak position of PL from type II QD heterostructures. PL from GaSb/GaAs QDs was blueshifted. Figue 3 shows this blueshift occurring in PL from GaSb/AlGaAs QDs. This revealed that GaSb/AlGaAs QDs has type II band alignment.

QD solar cells fabricated with GaSb/AlGaAs QDs revealed higher open circuit voltage and smaller short circuit current compared to that with GaSb/GaAs QD solar cells. This is explained by the higher band gap of AlGaAs and poor escape of photogenerated holes from the QDs due to an increase in the confinement energy.

Photocurrent spectroscopy at room temperature demonstrated the absorption of photons with energies below the band gaps of GaAs (1.5 eV) and AlGaAs (1.8 eV) corresponding to the QDs and wetting layers. The photocurrent decreased with increasing voltage, presumably due to the bias dependence of the escape efficiencies of holes from the QDs.

To observe two-step photocurrent, we used a 600 nm (2.1 eV) halogen lamp and a 1.55 μm (0.8 eV) laser. The lamp creates electron-hole pairs, whereas the 1.55 μm laser generates no carrier. Upon illumination with the laser, an increase in photocurrent, ΔI, was observed in solar cells fabricated from GaSb/GaAs QDs and GaSb/AlGaAs QDs (see Figure 4).

Conclusions and Future Work:

We successfully fabricated solar cells with ten layers of GaSb QDs embedded in GaAs and AlGaAs. We determined that GaSb/AlGaAs QDs has type II band alignment. We observed photocurrent generated from the QDs and wetting layers in both GaSb/GaAs QDs and GaSb/AlGaAs QDs, and analyzed the current-voltage characteristics. We observed two-step photocurrent generation, the key operating mechanism for IBSCs. We observed reduced photocurrent by changing the barrier from GaAs to AlGaAs, which is explained by strong confinement in GaSb/AlGaAs QDs. These results demonstrate the potential of GaSb/AlGaAs QD solar cells in realizing ideal IBSC and overcoming the SQ limit.

Future work includes investigating the dependence of the two-step process on incident laser power among other experiments to study the fundamental physics of GaSb/AlGaAs QD solar cells.

Acknowledgements:

I would like to thank my principal investigators, Drs. Noda and Sakaki, mentor, Dr. Elborg, and the High Efficiency Solar Cell/Quantum Nanostructures Group for their great assistance and patience; and the National Institute of Materials Science, National Nanotechnology Infrastructure Network International Research Experience for Graduates (NNIN iREG) Program, and National Science Foundation for making this research possible.

References:

[1] A. Luque and A. Martí. "Increasing the Efficiency of Ideal Solar Cells by Photon Induced Transitions at Intermediate Levels"; Physical Review Letters, v. 78, p. 5015-5017 (1997).

[2] P.D. Hodgson, et al. "Blueshifts of the Emmission Energy in Type II Quantum Dot and Quantum Ring Nanostructures"; Journal of Applied Physics, v. 114, p.1-6 (2012).

PHYS

A Coupled Dipole Approach to Electron Energy Gain Spectroscopy

Jacob Busche
Physics, Oregon State University

NNIN REU Site: Washington Nanofabrication Facility & Molecular Analysis Facility, University of Washington, Seattle, WA
NNIN REU Principal Investigator: Dr. David J. Masiello, Department of Chemistry, University of Washington
NNIN REU Mentors: Nichloas W. Bigelow and Steven C. Quillin, Department of Chemistry, University of Washington
Contact: buschej@onid.orst.edu, masiello@u.washington.edu, bigelow@u.washington.edu, quills@u.washington.edu

Abstract:

Electron energy gain spectroscopy (EEGS) is a spectroscopic technique designed to provide high-resolution imaging of metal nanoparticles and their collective electronic oscillations called plasmons. The EEGS procedure involves pumping a plasmon with a continuous or pulsed light source from a laser, passing a high-energy (~ 100 keV) electron beam generated within a scanning transmission electron microscope (STEM) near the nanoparticle, and observing the energy lost or gained by the electron as a result of its interaction with a plasmon. The primary directive of this project is to produce a numerical model of an EEGS experiment to simulate and predict the new spectral and spatial information content contained within it. A plasmon resonance peak was observed during simulations using this technique, suggesting electron energy gain can provide a viable, zero-loss peak independent method for probing the electronic behavior of metal nanoparticles.

Introduction and Procedure:

An EEGS simulation is conducted by using a coupled dipole or discrete dipole approximation (DDA) method that assumes the target nanoparticle is composed of a large number of individual polarizable points that interact with external electric fields. The nanoparticle is then driven by both a laser and a STEM in a numerical simulation, and the induced or scattered electric field of the nanoparticle is calculated as the matrix of dipole moments in the target is allowed to relax into a energy-favorable self-consistent state. The electric field of the laser is approximated by a monochromatic plane-wave, and at the sub-wavelength scale of the nanoparticle target, is taken to be constant.

A second order interaction between the photon field of the laser light and the electron beam from the STEM becomes possible due to the plasmon oscillation coupling with both forms of radiation. A probability of photon energy transfer is generated that is proportional to the product of the electric fields and polarizations due to both the plane-wave and electron beam interactions [1], and a plot can be generated for each target arrangement to determine the normalized loss probability for each photon of energy gained by a passing electron. The numerical experiment can produce energy-gain spectra for particles of varying geometry between ~ 10 nm and ~ 100 nm in length along any given axis, providing a tool for probing interesting nanoparticle arrangements.

EEGS was developed from; (1) earlier simulations performed by B. T. Draine [2] that used the DDA to determine plasmon resonance peaks under excitation from plane-wave monochromatic light only, and (2) electron energy loss spectroscopy (EELS) simulations performed by N. W. Bigelow and A. Vaschillo, which described the energy loss probability of passing electrons to an unexcited target. EEGS is designed to probe the plasmon-electron interaction probabilities at specific energies given by the plane-wave excitation of the system, thus freeing the results from uncertainty derived from the zero-loss-peak of a STEM [3].

Results:

The preliminary numerical experiments performed in this study modeled a spherical silver nanoparticle with a 15 nm diameter and dipole moments spaced at 1 nm. A typical plasmon peak was observed at 3.42 eV, which agreed well with the plasmon resonance spectrum generated by DDA and EELS simulations. The expression determining the gain probability was incomplete at the time of the simulation, although the data shown in the figure are correct up to a scaling factor. However, the large degree of qualitative agreement between the EEGS results and those of DDA and EELS show that electron energy gain spectroscopy can produce accurate and interesting new results in metal nanoparticle systems.

Future Work:

The energy gain probability expression in EEGS will be further refined, and the energy gain spectra from new simulations will be compared with known results from DDA and EELS methods to determine the accuracy of the technique. Numerical experiments on targets of interesting geometry will follow, probing the natural plasmon frequencies of nanoparticle systems that appear in active research.

PHYS

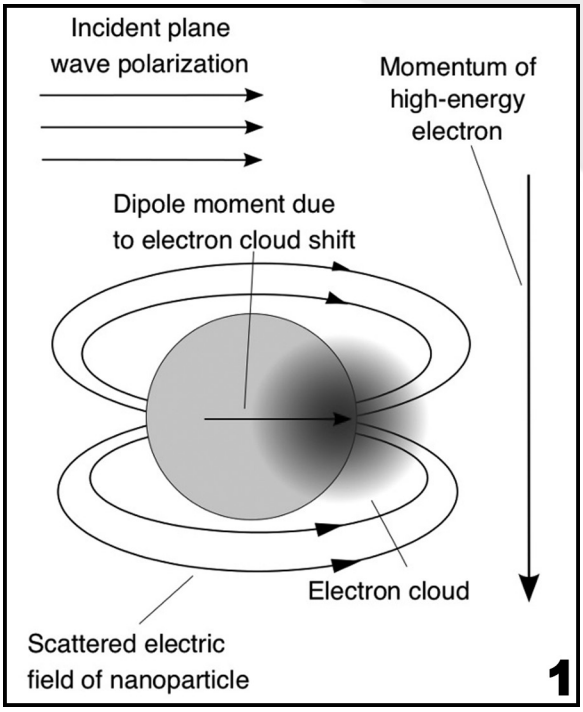

Figure 1, above: Experimental setup used to construct a typical EEGS simulation.

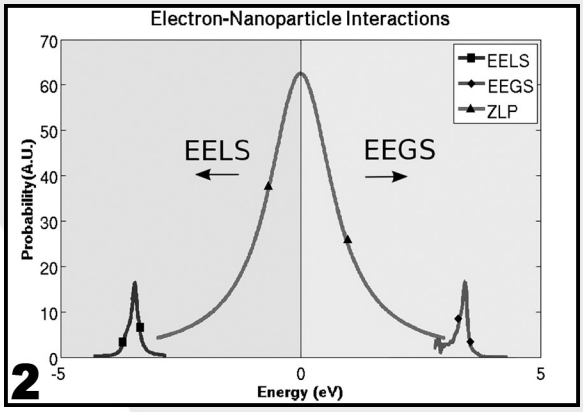

Figure 2, top right: The probability of energy loss or gain of a high energy electron passing a nanoparticle. The central zero-loss peak is described by a Lorentzian distribution.

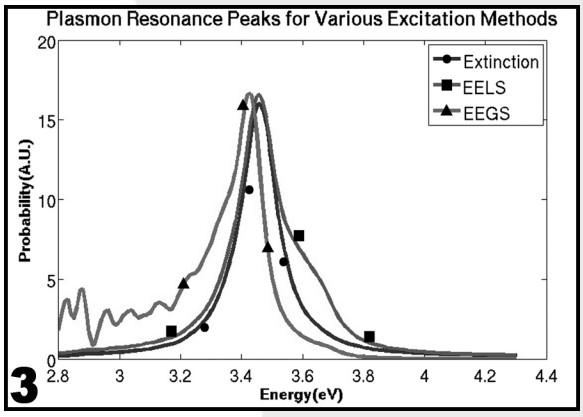

Figure 3, middle right: Typical plasmon resonance peaks are shown in DDA, EELS, and EEGS spectroscopies computed via the DDA.

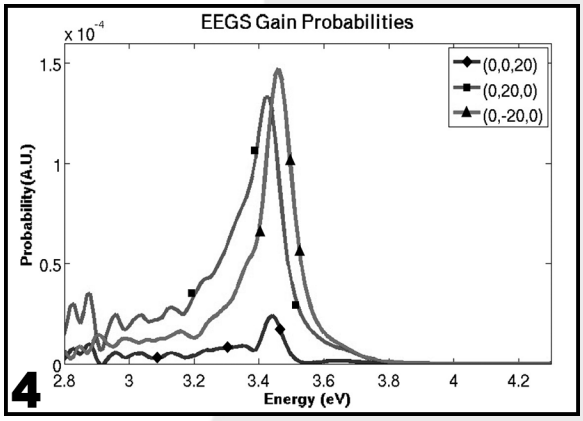

Figure 4, bottom right: The energy gain probability at several locations using EEGS. Both electrons and light propagate in the positive x-direction, with light polarized in the positive y-direction.

Acknowledgments:

I would like to thank Dr. David Masiello for welcoming me into his group and teaching me so much in such a short period of time. I would also like to thank Steven Quillin and Nicholas Bigelow for introducing me to their research and mentoring me through the rough patches, Niket Thakkar and Dr. Charles Cherqui for showing me how much fun the pursuit of knowledge can be, Paul Newbert for his instrumental assistance in life outside of research at this program, and the NNIN REU Program and the NSF for their support and funding of this great opportunity.

References:

[1] Arseño-Garcia, A. and García de Abajo, F. J.; "Discrete-dipole approximation for scattering calculations"; New Journal of Physics 15, 103021, 16 pp (2013).

[2] Draine, B. T. and Flatau, P. J.; "Discrete-Dipole Approximation for Scattering Calculations"; Journal of the Optical Society of America A Vol.11, No. 4, 1491-1499 (1994).

[3] Bigelow, N. W.; Vaschillo, A.; Iberi, V.; Camden, J. P.; Masiello, D. J.; "Characterization of the electron-and photon-driven plasmonic excitations of metal nanorods"; ACS Nano Vol.6, No. 8, 7497-7504 (2012).

PHYS

Fabricating Heavy Metal/Ferromagnetic Bilayers for Spin Torque Applications

Austin Little
Applied Physics, Morehouse College

NNIN REU Site: Cornell NanoScale Science & Technology Facility, Cornell University, Ithaca, NY
NNIN REU Principal Investigator: Prof. Daniel Ralph, Department of Physics, Cornell University
NNIN REU Mentor: Alex Mellnik, Department of Physics, Cornell University
Contact: austinjlittle@gmail.com, arm282@cornell.edu, dcr14@cornell.edu

Abstract:

Magnetic devices are leading contenders for future non-volatile memory and logic implementations. Applications for magnetic devices will require the development of efficient mechanisms for reorienting their magnetization. Spintronic devices use spin currents to exert a torque on the ferromagnetic layer, causing its magnetization to reorient. When a charge current flows through a metal with a strong spin-orbit coupling, the Spin Hall Effect creates a spin current transverse to the charge current direction. This spin current applies a torque to an adjacent ferromagnet. Topological insulators, which have surface states with large in spin-orbit coupling effects, are promising options for spin current sources. Previous research has shown that the topological insulator bismuth selenide (Bi_2Se_3) efficiently generates spin currents. However, due to the high resistivity of Bi_2Se_3, much of the charge current in a Bi_2Se_3/Permalloy devices flows through the low resistivity Permalloy (Py) and does not contribute to the torque. This issue can be resolved by using an insulating ferromagnet. We are working to develop a new method capable of measuring spin torques acting on insulating ferromagnets by using waveguide spin pumping and a Magneto-Optical-Kerr-Effect (MOKE) microscope. We will present initial measurements of Pt/Py test devices from the MOKE microscope.

Introduction:

In previous research [1], samples consisted of 8 nm of Bi_2Se_3 and 8 nm of Py patterned into strips 10-80 μm long and 2.5-24 μm wide, with an oxidized aluminum cap to prevent oxidation of the Py layer. Although the sample geometry produced measureable spin torques, on average Bi_2Se_3 was twenty-five times more resistive than Py. As a result, much of the current shorted through the Py layer and did not contribute to the spin torque.

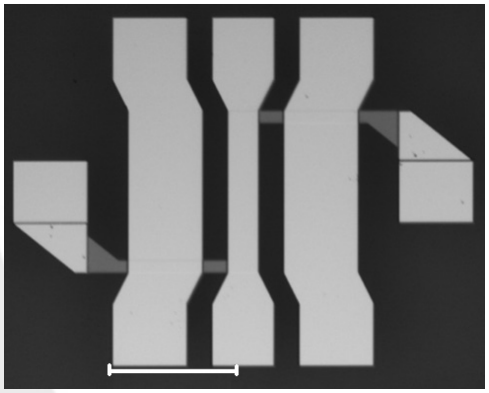

Figure 1: Device schematic.

Our current research involved new sample geometry where we deposited a hafnium oxide insulating ferromagnetic layer in addition to transmission waveguides. The hafnium oxide insulating ferromagnetic layer should prevent the current from shorting the Py layer, while the transmission waves guides should provide a general spin torque measurement.

To measure the vector components ($\parallel$, "in-plane") and ($\perp$, "perpendicular") of the spin torque, we also fabricated MOKE devices. The polarized light reflecting from our magnetic sample will image the scanned area and provide these vector components.

Experimental Procedure:

To make these devices, we began by depositing 6 nm of Pt and 6 nm of Py on a two-inch sapphire wafer. We also deposited 2 nm of aluminum oxide to prevent the Py from oxidizing. We then employed optical lithography and ion milling techniques to pattern the Pt/Py bilayers. We made electrical contacts from 3 nm of Ti and 150 nm of Pt in a symmetrical geometry, so that when samples were contacted using a ground-signal-ground high-

PHYS

frequency probe, the currents travelling in the contacts did not produce a net Oersted field acting on the sample.

To pattern the transmission waveguide devices, we used atomic layer deposition to deposit 18 nm of hafnium oxide to prevent current from entering the ferromagnetic layer, and deposited 3 nm of Ti and 150 nm of Pt for the actual waveguide devices.

Results and Conclusions:

Preliminary resistance measurements were taken on the devices to test the sample geometry. From these measurements, the sample geometry will be reconstructed where needed in order to prevent the current from shorting through the Permalloy layer and not contributing to the spin-torque.

Future Work:

In the near future, more measurements will be taken on the devices. One set of measurements will use radio frequencies to measure the components of the spin torque produced while the MOKE will measure an overall spin torque for the device.

Acknowledgements:

I would like to acknowledge my principal investigator Dan Ralph as well as mentor Alex Mellnik. I would also like to acknowledge Jonathan Gibbons for his extensive efforts in helping with the research this summer. I thank the National Nanotechnology Infrastructure Network Research Experience for Undergraduates (NNIN REU) Program and NSF for funding. Lastly, I would like to thank Melanie-Claire Mallison and the CNF staff for their support.

References:

[1] Spin-transfer torque generated by a topological insulator; A. R. Mellnik, J. S. Lee, A. Richardella, J. L. Grab, P. J. Mintun M. H. Fischer, A. Vaezi, A. Manchon, E.-A. Kim, N. Samarth, and D. C. Ralph. Nature 511, 449-451, (24 July 2014). doi:10.1038/nature13534.

PHYS

Fabrication of Nanoholes Smaller than 100 Nanometers

Luke Ness
Applied Physics and Computer Science, Bethel University

NNIN REU Site: Minnesota Nano Center, University of Minnesota-Twin Cities, Minneapolis, MN
NNIN REU Principal Investigator: Dr. Sang-Hyun Oh, Electrical and Computer Engineering, University of Minnesota-Twin Cities
NNIN REU Mentors: Daehan Yoo and Xiaoshu Chen, Electrical and Computer Engineering, University of Minnesota-Twin Cities
Contact: lan77962@bethel.edu, sang@umn.edu, yooxx094@umn.edu, chenx604@umn.edu

Abstract:

Nanohole arrays patterned in noble metal films can function as optical biosensors, because the extraordinary optical transmission through the nanoholes changes sharply with refractive index changes near the metal surface. Smaller nanoholes have sharper resonance peaks, making a better sensor. At the same time, smaller nanoholes have lower transmission efficiency. Template-stripped silver (Ag) nanohole arrays of varying diameters were used in combination with an ultra bright white light source to look at the difference in the optical response of nanoholes with diameters below 100 nm.

Experimental Procedure:

To achieve the resolutions needed for the nanohole arrays, electron-beam lithography was used to pattern thermally grown silicon dioxide (SiO_2) on a silicon wafer. The cost and speed of using electron-beam lithography limited the arrays size to be too small for practical biosensing applications. After the electron-beam resist was patterned and developed, a reactive ion etcher was used to etch through the SiO_2 layer. Images of the mold were taken to measure the hole size using a scanning electron microscope (SEM) before metal deposition, as shown in Figure 1. The SiO_2 layer was then used as a mask for etching into the Si wafer creating a mold for nanohole arrays; 100 nm of Ag was then deposited onto the mold using an electron-beam evaporator. The use of electron-beam deposition was important because the sides of the nanoholes in the silicon mold cannot have metal deposited on them otherwise they would close up and the nanoholes would not appear.

The deposited Ag was adhered to a glass slide with epoxy. The glass slide was then peeled off the silicon mold, creating template-stripped Ag nanohole arrays with ultra-smooth metallic surface. The Ag nanohole arrays were then imaged again with a SEM, as shown in Figure 2. The diameters of the nanohole arrays were found to be 53 and 105 nm.

Using a broadband fiber-coupled, laser-driven light source with a 300 mm focal length imaging spectrometer, the spectrums emitted by both nanohole arrays were recorded as shown in Figure 3. The spectrums from the nanohole arrays were normalized with the spectrum of light transmitted through the glass slide. Mixtures of glycerol and water were used to measure the sensitivity of the nanohole arrays to the change to the refractive index on the exposed side of the array.

Results and Discussion:

The percent of transmitted light dropped by half an order of magnitude for the 53 nm holes compared to the 105 nm holes. The spectrums then had an eighth order polynomial fitted to them. This equation was used to find the maximum value of the fourth peak and the spectral shift was plotted for each refractive index as shown in Figure 4. The sensitivity of the two arrays was 517.33 nm/RIU for the holes with a diameter of 53 nm and 505.89 nm/RIU for the holes with a diameter of 105 nm. The data in Figure 4 was expected to be linear and was with the exception of the fourth data point in both of the data sets. The cause behind this abnormality was not able to be rectified because of time constraints.

Full width at half maximums (FWHMs) were approximated to evaluate the sharpness of the fourth peaks. The FWHMs was about 10 nm for the holes with a diameter of 53 nm and about 16 nm for the holes with a diameter of 105 nm. Making nanohole arrays with a smaller hole size is an easy way to improve the sensitivity and sharpness of the resonant peaks. Making holes below 100 nm is only a useful technique if you have an ultra bright light source, such as the laser driven light source that was used in this experiment. This is because of the extremely low transmittance through these nanohole arrays.

The improved sensitivity and sharpness of holes below 100 nm can allow for biosensing experiments that need higher precision.

PHYS

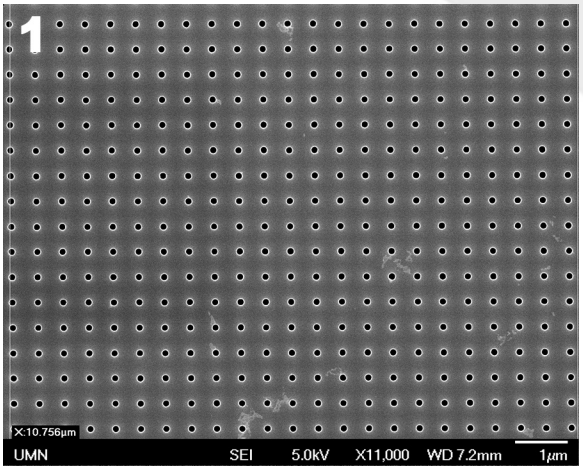

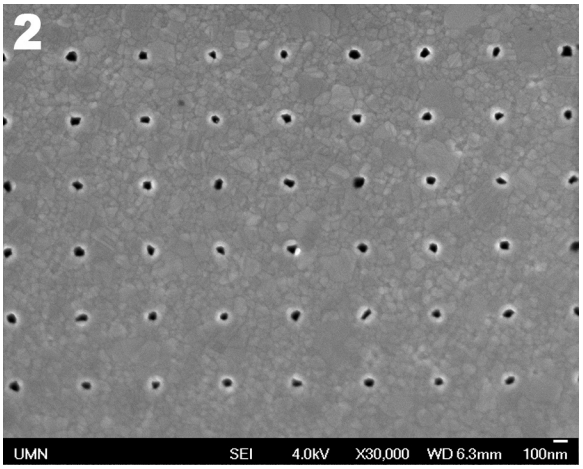

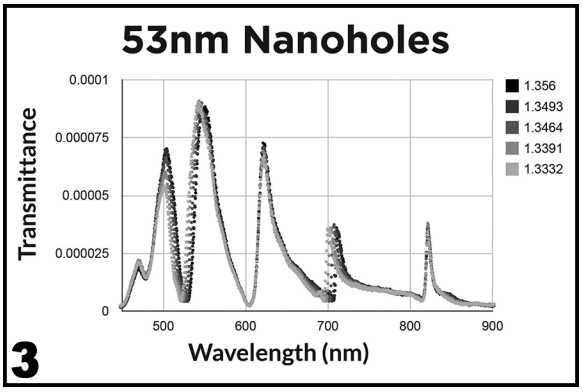

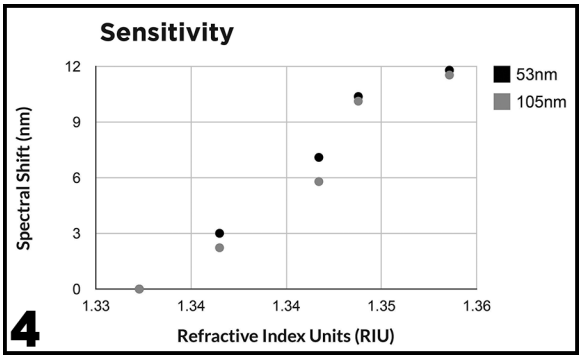

Future Works:

The next step for nanohole arrays with diameters below 100 nm is to create them on a larger scale with methods such as nanoimprinting. This will allow the arrays can be used as an actual sensor. The uniformity of the nanoholes also increase by a considerable degree from the silicon molds to the template-stripped Ag nanohole arrays. Using electron beam lithography to make smaller initial holes while depositing less metal could improve these sensors as well.

Acknowledgements:

I would like to thank Dr. Sang-Hyun Oh for allowing me to be a part of his lab throughout this summer and the guidance that he gave for my research. I would also like to thank Xiaoshu Chen and DaeHan Yoo for teaching me the techniques in the cleanroom that I used throughout the summer as well as the basics behind nanoplasmonic devices. This project would have not been possible without the support of the Minnesota Nano Center and the National Nanotechnology Infrastructure Network Research Experience for Undergraduates (NNIN REU) Program. Finally I would like to thank the National Science Foundation for funding this research.

Figure 1, top left: SEM image of bare silicon with 117 nm holes in it.

Figure 2, upper left: SEM images of template-stripped Ag with 53 nm holes in it created from the silicon mold with 117 nm holes.

Figure 3, lower left: Plot of the spectrum of light emitted from the 53 nm holes.

Figure 4, bottom left: Shows the change in the resonant frequency of the fourth peak against the change of the refractive index of the fluid.

PHYS

Growth and Transfer of 2D Semiconductors and Heterostructures

Nicholas Stone-Weiss
Physics, Juniata College

NNIN REU Site: Washington Nanofabrication Facility & Molecular Analysis Facility, University of Washington, Seattle, WA
NNIN REU Principal Investigator: Xiaodong Xu, Department of Physics, University of Washington
NNIN REU Mentor: Genevieve Clark, Department of Materials Science and Engineering, University of Washington
Contact: stonenm11@juniata.edu, xuxd@uw.edu, gcl4rk@gmail.com

Abstract:

Physical vapor transport (PVT) was utilized to grow two-dimensional (2D) semiconductors that can be used in devices such as transistors, LEDs, and solar cells. Molybdenum diselenide ($MoSe_2$), which is in the transition metal dichalcogenide (TMDC) family, was the main semiconductor grown during this study. Limited numbers of papers have been released in which $MoSe_2$ monolayer crystals have been grown via PVT. In this study, $MoSe_2$ and other TMDC thin flakes are grown onto a SiO_2 on silicon substrate in a high-temperature furnace using PVT. Monolayer crystals were distinguished and characterized by optical imaging, photoluminescence measurements, and atomic force microscopy. By spin-coating poly(methyl methacrylate) (PMMA) onto the growth substrate, we were able to transfer the as-grown samples successfully. The PVT methods explored in this study can be further developed to create either lateral or vertical heterostructures between different monolayers.

Introduction:

Two-dimensional (2D) semiconductors have been studied extensively in recent years, as their 2D nature can make semiconductor properties easier to control. Along with their unique characteristics, 2D semiconductors are more flexible and cheaper to produce than traditional semiconductors [1]. Following the exfoliation of graphene that won the Nobel Prize in 2010, further methods of creating 2D semiconductors were developed to improve semiconductor yield and accelerate production of viable results [1]. Graphene, lacking a naturally existing band gap, began to be looked past for use in electronic devices due to the necessity of a band gap [1, 2]. Transition metal dichalcogenides (TMDCs) are 2D materials with an existing band gap having electrical properties that can improve upon graphene. Exfoliation via the Scotch tape method has proven successful for the creation of monolayer TMDCs, however the process is also time-consuming and yields few viable 2D semiconductors quickly [2]. PVT has emerged as a new technique for synthesizing 2D materials in a more time-efficient manner.

PVT involves the use of a high-temperature furnace to deposit crystalline monolayer materials onto a substrate. TMDCs have a hexagonal lattice with the form MX_2 ("M" being a transition metal and "X" a chalcogenide) [3]. Molybdenum diselenide ($MoSe_2$) and tungsten diselenide (WSe_2) are two TMDCs explored due to their ideal band gap for electronic circuit applications. $MoSe_2$ in particular has a direct band gap of 1.5 eV as well as a drastic photoluminescence change when in monolayer form, making it suitable for use in LEDs and solar cells [2]. Finding a consistent method for creating monolayer TMDCs can have various useful electronic applications.

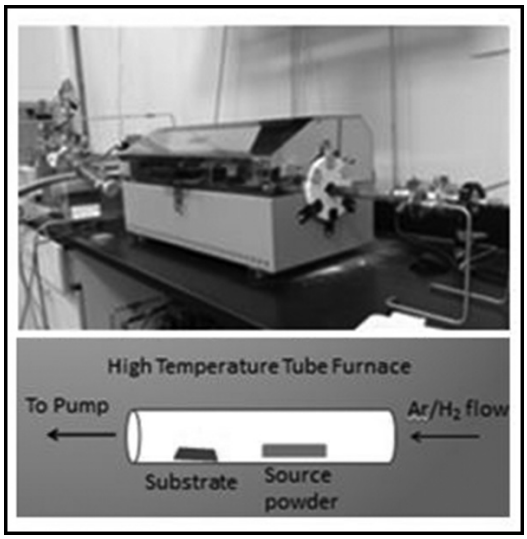

Figure 1: (a) PVT furnace setup used to grow TMDCs. (b) Diagram of setup within furnace

Methods:

Using the setup shown in Figure 1, monolayer $MoSe_2$ was grown. A mixture of $MoSe_2$ and MoO_3 powder was placed inside the furnace as the source. SiO_2 on an Si substrate was placed upstream from the source powder in a temperature gradient. The furnace was steadily heated to a growth temperature of between 830 and 900°C at 100 millitorr. Once the maximum

PHYS

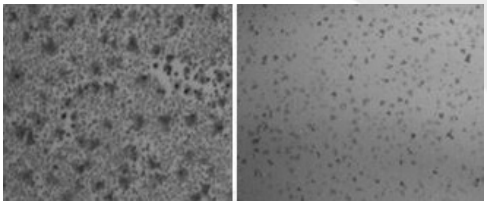

Figure 2: (a) Monolayer and bilayer $MoSe_2$ growth. (b) Monolayer triangular growth.

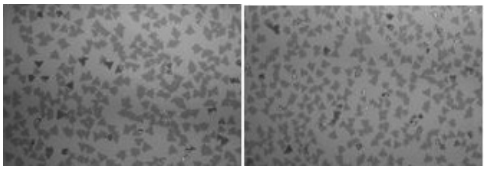

Figure 3: (a) Pre-transferred growth. (b) Post-PMMA transferred growth on new substrate.

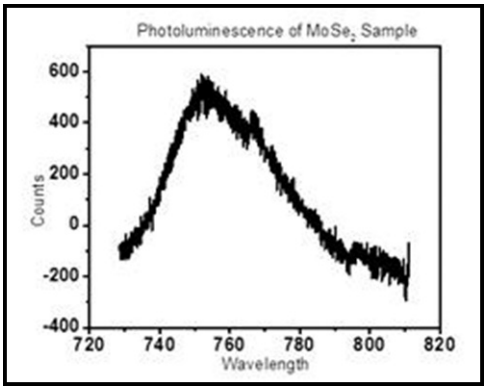

Figure 4: PL Spectrum of $MoSe_2$ sample.

temperature was reached, argon and hydrogen gas were flown for five minutes at 70-100 sccm and 10-27 sccm, respectively. Following the growth period, the furnace was steadily cooled to room temperature.

Monolayer $MoSe_2$ was successfully grown, however results were inconsistent. Photoluminescence (PL) measurements verified the presence of monolayer crystals; however the PL peak was shifted from an expected $MoSe_2$ peak. Crystalline triangles of monolayer $MoSe_2$ were found at multiple parameters, but results were not repeatable. We attributed the PL peak difference to crystalline impurity due to growth parameters not being optimized.

Improving upon growth parameters will lead to more reliable results that can vastly improve upon exfoliation with regard to monolayer yield. Increasing the triangle size will also improve our ability to use monolayer $MoSe_2$ in devices.

Monolayer TMDC growth was transferred off the growth chip by spin-coating PMMA and etching in 1 M KOH solution. A thin film of PMMA containing growth was transferred onto a new substrate and cleaned with a series of solvent baths. Although optical microscopy verified the success of PMMA transfer, AFM images exposed impurities in transferred growth. In the future, dry transfer methods will be explored that cause less damage to the growth.

Conclusions and Future Directions:

Monolayer $MoSe_2$ was successfully grown, however results need to be replicated to make these 2D semiconductors viable. Triangular crystals need to be optimized so that they are large enough for utilization in devices, as $MoSe_2$ has highly attractive electronic properties. With the development of successful monolayer growth, establishment of an effective dry transfer technique can help create vertical heterostructures between TMDC monolayers that are necessary for devices. Similarly, using PVT and known parameters for other TMDCs, lateral heterostructures may be grown between 2D materials with similar lattice structures [3], which would create a 1D quantum wire with interesting electronic properties [4].

Acknowledgements:

Genevieve Clark, Xiaodong Xu, Marie Scott, Kyle Seyler Xu Lab Group, Nanodevice Physics Lab Group, National Nanotechnology Infrastructure Network Research Experience for Undergraduates (NNIN REU) Program, National Science Foundation, and University of Washington.

References:

[1] Editorial, Graphene is not alone, Nature Nanotechnology, 7, 2012, 683.

[2] Xia, J., Huang, X., Liu, L., Wang, M., Huang, M., Zhu, D., Li, J., Gu, C., and Meng, X., CVD synthesis of large-area, highly crystalline $MoSe_2$ atomic layers on diverse substrates and application to photodetectors, Royal Society of Chemistry, 2014, 6, 8949-8955.

[3] Huang, C., et al., Lateral heterojunctions within monolayer semiconductors, 1-26 (2014) at <http://arxiv.org/ftp/arxiv/papers/1406/1406.3122.pdf>

[4] Sone, J., Electron transport in quantum wires and its device applications, Semiconductor Science and Technology. 7, B210 (1992).

PHYS